Dissipation in granular materials

Dietrich E Wolf, Farhang Radjai, Sabine Dippel

Dissipation in granular materials

By Dietrich E. Wolf †, Farhang Radjai and Sabine Dippel

Theoretische Physik, Gerhard-Mercator-Universität Duisburg,
D-47048 Duisburg, Germany

Abstract

For two simple set-ups, we discuss how dissipative grain–grain interactions give rise to unexpected properties on large scales. In the first example, a spherical particle rolling along a rough surface experiences an effective viscous friction on large time scales. It is due to temporal correlations among collisions with incomplete normal restitution. The second example is a sheared granular packing. There, spatial correlations among non-sliding and sliding contacts with Coulomb friction suggest that the deviatoric stress, although responsible for the dissipation, is localized on bonds that are non-sliding and hence non-dissipative.

§ 1. Introduction

Granular media (such as sand) are classical many-particle systems with dissipative interactions (for a recent review see Jäger *et al.* (1996)). In the absence of external driving, the kinetic energy of the grains decreases in each collision owing to the irreversible transfer of energy into the internal degrees of freedom of the grains‡. This is called collisional cooling§. Often the grains form lasting contacts within a finite time, which is called inelastic collapse (McNamara and Young 1994). It happens if the relative velocity of the grains (i.e. the granular temperature) drops to zero, while the local pressure stays finite. An example is a heap of sand. The weight of the grains provides a finite pressure in the pile, while the collisional cooling eliminates all relative motion. That this happens within a finite time can easily be illustrated with a single steel ball bouncing back from a plane and losing a finite fraction of its kinetic energy with each collision. In the absence of a gravitational field the inelastic collapse may still happen in a finite region of the granular material if the outer regions provide enough pressure to compactify the inner part.

In order to keep granular media in a steady or periodic motion, the translational and rotational degrees of freedom of the grains have to be agitated externally. One can regard it as the second characteristic property, besides the dissipative interactions, distinguishing the class of granular materials from other many particle systems such as liquids or solids, that the typical agitation energy per degree of freedom has to be much larger than the thermal energy $k_B T/2$. A sand pile is frozen into a metastable configuration, for instance. In order to agitate any grain, a minimal

† e-mail:d.wolf@uni-duisburg.de

‡ The partial regain of translational energy from internal degrees of freedom has been discussed by Giese and Zippelius (1996) and leads to a stochastic restitution coefficient. This will not be considered further in this paper.

§ The term 'cooling' here refers to the so-called granular temperature which is the mean square deviation of the velocities from their average.

energy of the order of mgr is needed, where m and r denote the mass and radius respectively of a grain and g is the gravitational acceleration. For $r > 1\,\mu m$ this becomes larger than the thermal energy of room temperature. Therefore, for example Brownian motion is unimportant for granular media. In so-called dry granular media, cohesion and hydrodynamic interactions can also be neglected. This is the case considered in this paper.

Two types of irreversible interaction model are important in granular materials. There is on the one hand the incomplete normal restitution in head-on collisions. The corresponding phenomenological material parameter is the normal restitution coefficient

$$e_n = \left| \frac{v_f}{v_i} \right| < 1, \tag{1}$$

which is the ratio of the relative velocities after and before the collision. It is smaller than unity, because a fraction $1 - e_n^2$ of the kinetic energy is irreversibly lost to internal degrees of freedom of the grains.

On the other hand, there is energy dissipation during a sliding contact due to Coulomb friction, at a rate $F_t v_t$. The friction force F_t is proportional to the normal force F_n pressing the grains together. The dynamic friction coefficient is the ratio of the two forces:

$$\mu_d = \left| \frac{F_t}{F_n} \right|. \tag{2}$$

Of course, these dissipative grain–grain interactions characterized by equations (1) and (2) are idealized (see for example Schäfer *et al.* (1996) and Baumberger and Berthoud (1997) for refinements), but they are legitimate starting points for elucidating the dissipation phenomena on large scales, which is the aim of this paper.

In general the dissipation in a granular material is dominated by only one of these two irreversible grain–grain interactions. For example, Coulomb friction is unimportant as a source of dissipation in a granular gas, where the dynamics are mostly due to binary collisions. On the other hand, the plastic deformation of granular packing involves almost exclusively sliding of particles with respect to each other, so that the incomplete normal restitution in the few collisions contributes only very little to the overall dissipation.

Accordingly we present the following two examples: the first in which the incomplete normal restitution is the microscopic source of dissipation, and the second in which the Coulomb friction is the microscopic source of dissipation. In both examples the dissipation on large scales shows qualitatively new features which are not obvious from the microscopic laws. The incomplete normal restitution gives rise to a velocity-independent ('viscous') friction for a sphere rolling along a rough surface, and the Coulomb friction leads to a localization of dissipation on a small fraction (about 8%) of contacts, when a granular packing is plastically deformed.

§2. Why surface roughness causes viscous friction for a rolling sphere

The first example is a spherical particle rolling down a rugged incline consisting of small spheres itself (figure 1). Here we only summarize the results for two dimensions (Ancey *et al.* 1996, Dippel *et al.* 1996). The mechanism leading to the effective friction is very similar in three dimensions (Dippel *et al.* 1997). For simplicity we

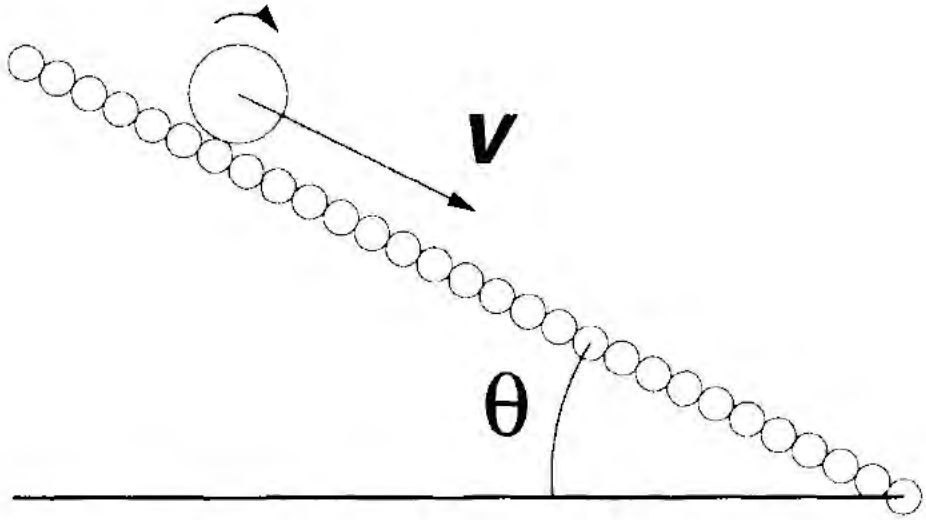

Figure 1. A sphere rolling along a rugged surface experiences an effective viscous friction.

assume that the spheres of the incline are densely packed. More general situations have been investigated and do not lead to any important differences (Dippel *et al.* 1996).

2.1. *Velocity–force diagrams*

Let us first consider three simpler cases. A sphere rolling down a plane accelerates. It never reaches a steady state. By contrast, a solid block sliding down the tilted plane may reach a steady state, albeit a trivial one. If the inclination is small enough, the block simply stops sliding. If the driving force $F = mg \sin \theta$ exceeds the Coulomb friction force, however, the block will accelerate for ever. Figure 2 shows the Coulomb graph, which allows one to read off the points (v, F) for which a steady state with velocity v and driving force F (which of course is compensated by the friction force in a steady state) exists. These points lie on the bold lines. All other points (v, F) do not correspond to a steady state but evolve in time along the broken flow lines. For example, for $v = 0$ any driving force smaller than F_s will be compensated by static Coulomb friction. However, for a driving force $F > F_s$ the block will start to slide and be accelerated with the force $F - F_d$.

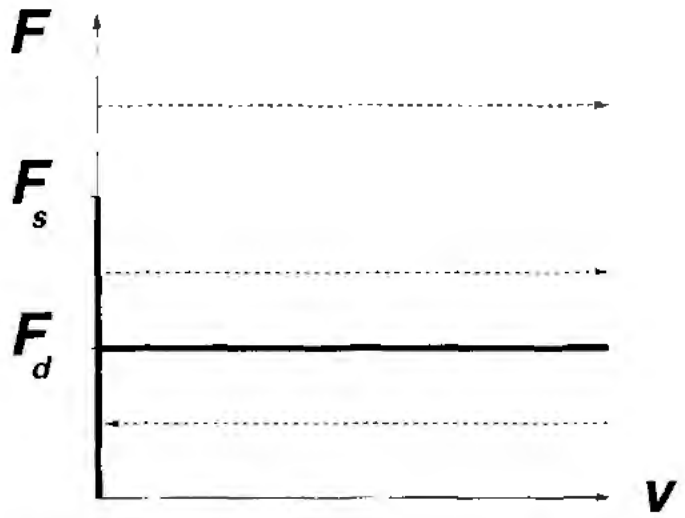

Figure 2. The points (v, F) on the bold lines correspond to steady states of a solid block subject to Coulomb friction. For fixed driving force the velocity evolves along the broken lines.

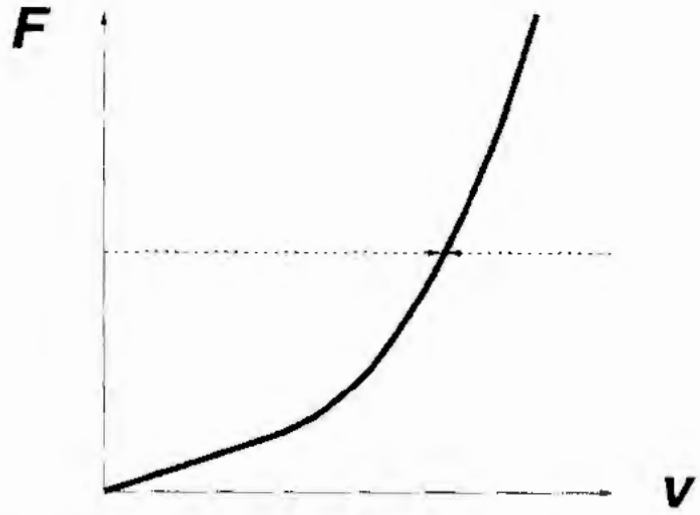

Figure 3. Frictional force F of a sphere moving with velocity v in a viscous medium. For fixed driving force the velocity evolves along the broken line.

The Coulomb graph should be contrasted with the corresponding diagram for viscous friction (figure 3). A sphere falling in a viscous medium experiences a frictional force which is linear for laminar and quadratic for turbulent flow. Here any driving force leads to a steady state. The velocity adjusts itself such that the viscous friction compensates the driving force.

Having a rugged instead of a flat incline, little as this change may seem, leads to a surprisingly rich velocity–force diagram (figure 4). There are at least three force intervals, separated by F_{AB} and F_{BC}. If the driving force $F < F_{AB}$, a sphere launched

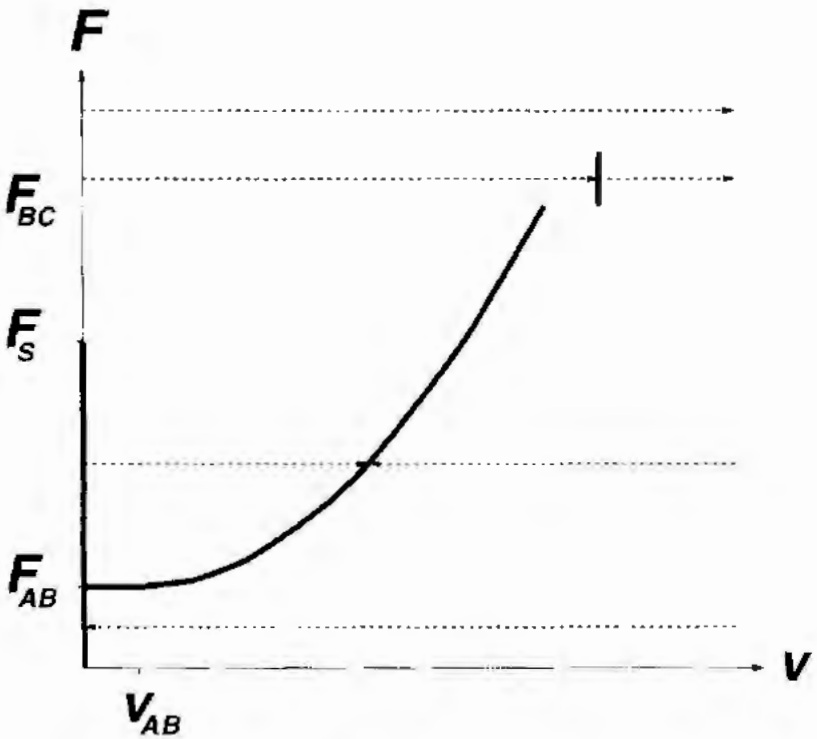

Figure 4. Schematic velocity-force diagram of a sphere rolling along a rugged surface. Velocity v averaged over duration of the contact with one surface sphere. The bold lines correspond to steady states. Below a driving force F_{AB} the sphere stops rolling. Between F_{AB} and F_{BC} there exists a steady state with finite velocity. Above F_{BC} computer simulations indicate a force interval, for which a steady-state velocity can be reached from below, but not from above. For even larger driving force, no steady state is reached.

with any velocity v will become trapped, that is it stops rolling after passing a number of substrate spheres. If F_{AB} is exceeded and the initial velocity is large enough to go over the first little bump on the incline, the rolling sphere reaches a steady state. If the driving force is larger than F_{BC}, however, no stable state exists any longer, as indicated by the flow lines. The sphere starts to make larger and larger bounces. In the following we discuss the effective friction which guarantees a steady-state motion in the intermediate regime between F_{AB} and F_{BC}.

2.2. *The effective friction in the steady-state regime*

In a steady state the driving force F can be identified (apart from the sign) with an effective frictional force which describes the dissipation of the energy input. Molecular dynamics simulations (Wolf 1996) and experiments (Ristow *et al.* 1994) show that this effective frictional force depends on the velocity approximately like

$$F - F_{AB} \propto \frac{m}{r}(v - v_{AB})^2. \tag{3}$$

The offset v_{AB} is a function of the ratio of the radius R of the rolling sphere to the radius r of the surface spheres and approaches zero for increasing R/r (figure 5). Equation (3) means that the rolling particle effectively feels a viscous friction.

There is a second even more remarkable observation. The data for different restitution coefficients e_n (see figure 5) and also for different friction coefficients μ_d are indistinguishable. The effective friction depends very little on the material coefficients characterizing the dissipation on the scale of one grain.

These two key observations will now be explained qualitatively. A quantitative analysis will be given in the next section. For the explanation of equation (3) we may consider the limiting case $e_n = 0$, $\mu_d \to \infty$. Why equation (3) holds, no matter what the precise values of e_n and μ_d are, will be explained afterwards.

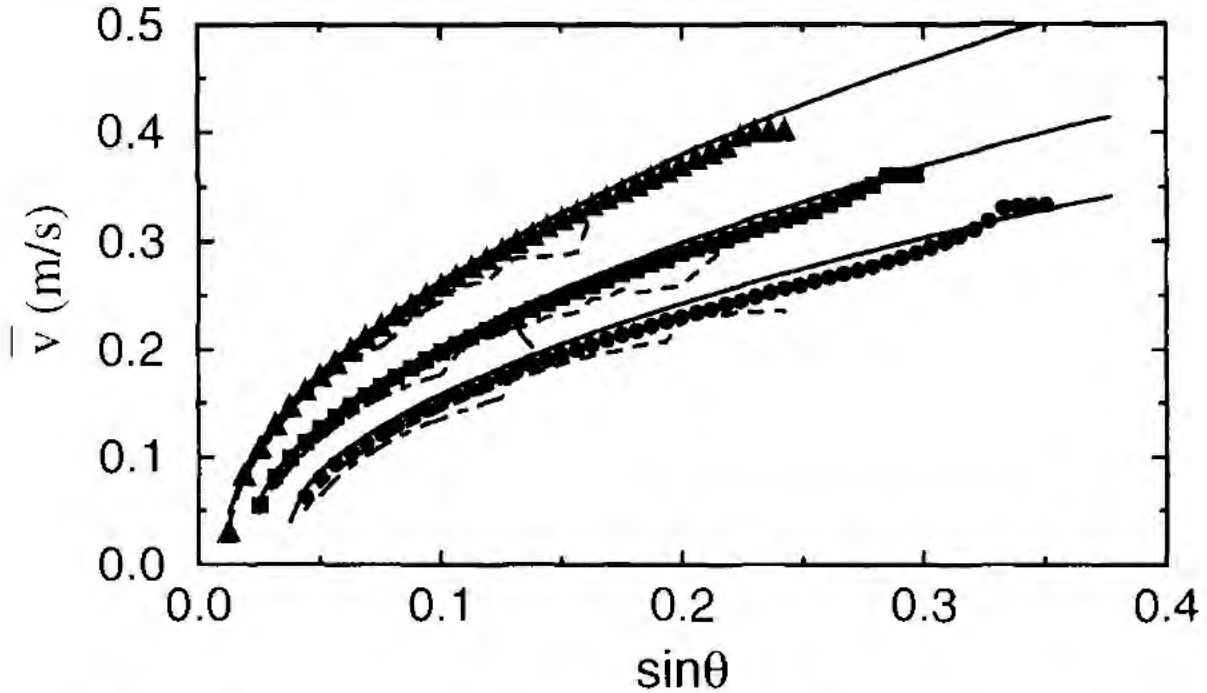

Figure 5. Simulation results of $\bar{v}$ as a function of the driving force $F = mg \sin\theta$. The ratio of the radius R of the rolling sphere to the radius r of surface spheres is $R/r = 1.75$ for the lowest curves (●), 2.25 in the middle (■) and 3 for the uppermost curves (▲). The data for $e_n = 0.7$ (- - - - -) and 0.5 (– – – –) are indistinguishable from those for $e_n = 0.1$ (●, ■, ▲). Also shown in the analytical prediction for $e_n = 0$ (—— –).

In this limiting case the motion becomes particularly simple. Because $\mu_d \to \infty$ the sphere has no slip relative to the bumps on the incline. It must roll without dissipation. The only dissipation happens when the rolling sphere first hits a new bump. Because $e_n = 0$, the kinetic energy stored in the motion perpendicular to the new bump surface is dissipated at once. The moving sphere does not bounce back. For simplicity we consider only the case when it stays always in contact with the inclined surface (no detachment due to centrifugal force).

The kinetic energy at any point on bump $k+1$ is related to that at the corresponding point on the preceding bump by

$$E_{\text{kin},k+1} = E_{\text{kin},k} + \Delta E_{\text{pot}} - \frac{m v_{\text{n,k}}^2}{2}. \tag{4}$$

The last term is the energy dissipated in one collision, and

$$\Delta E_{\text{pot}} = 2rF = 2rmg \sin\theta \tag{5}$$

is the difference in potential energy. Obviously, for a steady state, one must have

$$2rF = \frac{m v_n^2}{2} \equiv E_{\text{diss}}. \tag{6}$$

This explains why the effective friction has a quadratic velocity dependence.

Simple geometry (figure 6) shows that the normal component of the velocity v just before the collision with a new bump is

$$v_n = v \sin(2\gamma_{\max}), \tag{7}$$

where $\gamma_{\max} = \sin^{-1}[r/(R+r)]$. This explains why the steady-state velocity increases with increasing ratio $R/r > 1$ of the radii of the rolling sphere and those forming the incline (see figure 5). The larger the rolling sphere, the smaller is the normal component of its velocity, when it hits the new bump, and hence the less efficient is the dissipation.

With equations (7) and (6) and some elementary trigonometric transformations the steady-state velocity v just before the collision with a new bump is

$$v^2 = \frac{Fr}{mc(1-c)}, \qquad \text{with} \qquad c = \sin^2\gamma_{\max} = \left(\frac{r}{R+r}\right)^2. \tag{8}$$

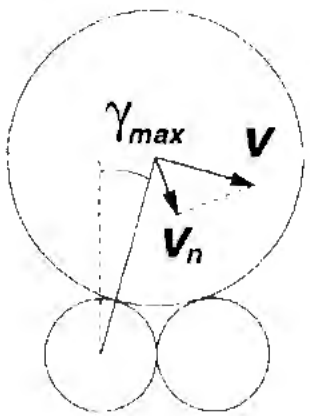

Figure 6. At angle $\gamma = \gamma_{\max}$ the rolling sphere hits a new substrate sphere and looses the normal component v_n of its velocity. The kinetic energy of the tangential motion is redistributed between the rotational and translational degrees of freedom.

In the next section we shall see that v is representative for the average velocity $\bar{v}$.

The surprising result that the effective friction force is nearly independent of the value of e_n can be understood in the following way. We found by computer simulation that a steady state requires essentially that the moving sphere undergoes an inelastic collapse on each substrate particle. One can assume that it has formed a lasting contact when it reaches the next substrate particle, with almost the same tangential velocity as in the case $e_n = 0$. Whether or not the inelastic collapse can be completed before the next surface bump is hit depends on the coefficient of restitution. Therefore F_{BC} is a function of e_n. Increasing e_n tends to destabilize the steady state. The results are independent of the friction coefficient μ_d, as long as the moving sphere rolls when it is in contact with the surface.

2.3. *Analytic calculation of the velocity–force diagram*

In order to show the stability of the steady state and to evaluate the average velocity, one needs to know the kinetic energy E_{kin} in equation (4). As the sphere is rolling, it rotates about its centre of mass with angular frequency $\omega = v/R$. The kinetic energy has a translational and a rotational contribution:

$$E_{kin} = \frac{mv^2}{2} + \frac{J\omega^2}{2} = \frac{m_{eff}v^2}{2} \tag{9}$$

with an effective mass $m_{eff} = m(1 + J/mR^2)$, where J denotes the moment of inertia. Hence equation (4) becomes

$$\frac{m_{eff}v_{k+1}^2}{2} = \frac{m_{eff}v_k^2}{2} + 2rF - 2mc(1-c)v_k^2. \tag{10}$$

The stability of the steady-state solution is now easily checked. Let $\Delta v_k^2 = v^2 - v_k^2$ denote the distance from the steady-state value. Then the iteration has the simple form

$$\Delta v_{k+1}^2 = \left(1 - \frac{E_{diss}}{E_{kin}}\right)\Delta v_k^2. \tag{11}$$

As E_{diss}/E_{kin} is smaller than unity, Δv_k converges to zero exponentially.

Now we use these results to determine the average velocity in the steady state. Knowing the velocity v at γ_{max} (see figure 6) any previous velocity $v(\gamma)$ can be obtained from energy conservation for $-\gamma_{max} < \gamma < \gamma_{max}$:

$$\frac{m_{eff}v^2}{2} = \frac{m_{eff}v^2(\gamma)}{2} + mg(r+R)[\cos(\theta+\gamma) - \cos(\theta+\gamma_{max})]. \tag{12}$$

Solving this for $v^2(\gamma)$, one obtains

$$v^2(\gamma) = v_0^2[b - \cos(\theta+\gamma)] = (R+r)\dot{\gamma} \tag{13}$$

with the characteristic velocity

$$v_0 = \left(\frac{2m}{m_{eff}}g(R+r)\right)^{1/2} \tag{14}$$

and the dimensionless constant

$$b = \left(\frac{v}{v_0}\right)^2 + \cos(\theta+\gamma_{max}). \tag{15}$$

The average velocity $\bar{v}$ is given by the arc length $2\gamma_{max}(R+r)$ divided by the duration T of the contact with one bump:

$$\bar{v} = \frac{2\gamma_{max}(R+r)}{T}. \tag{16}$$

Inserting equation (13) into

$$T = \int_{-\gamma_{max}}^{\gamma_{max}} d\gamma\, \dot{\gamma}^{-1}, \tag{17}$$

the average velocity (16) is determined by

$$\frac{v_0}{\bar{v}} = \frac{1}{2\gamma_{max}} \int_{\theta-\gamma_{max}}^{\theta+\gamma_{max}} \frac{d\gamma}{(b-\cos\gamma)^{1/2}}. \tag{18}$$

The integral in equation (18) is an elliptic integral of the first kind and cannot be solved in closed form. The theoretical curves in figure 5 are obtained by numerical evaluation of this formula and are in excellent agreement with the data.

However, one can get additional insight by expanding $\bar{v}$ for small r/R (or small c, (equation (8))), keeping the driving force F (i.e. the inclination θ) fixed. This is done in the appendix. The result is

$$\frac{m}{r}v^2 = F\left[\left(\frac{R}{r}\right)^2 + 2\frac{R}{r} + 2\left(1 - \frac{m}{m_{eff}}\right)\right] + O\left(\frac{r}{R}\right). \tag{19}$$

This specifies the proportionality constant in equation (3) and shows that the offsets vanish in the limit $r/R \to 0$.

Finally, we determine the value F_{AB} of the driving force, below which $\bar{v} = 0$ is the only steady state. The integral (18) is only finite if $b > 1$. It diverges for $b \to 1$ like $|\ln(b-1)|$, that is v vanishes like $1/|\ln(b-1)|$. We conclude that $b = 1$ implicitly determines F_{AB}. This can also be seen from equation (13). While rolling over a substrate sphere, the highest point ($\gamma = -\theta$) is reached with zero velocity, if $b = 1$.

Inserting equations (8) and (14) into equation (15), one finds that

$$b = a\sin\theta + (1-c)^{1/2}\cos\theta \tag{20}$$

with the abbreviation

$$a = \left(\frac{m_{eff}}{2m}\frac{1}{c(1-c)} - 1\right)c^{1/2}. \tag{21}$$

Substituting $b = 1$ and solving for $\theta_{AB} = \sin^{-1}(F_{AB}/mg)$, one obtains (see appendix)

$$\theta_{AB} = \sin^{-1}\left(\frac{1}{(a^2+1-c)^{1/2}}\right) - \tan^{-1}\left(\frac{(1-c)^{1/2}}{a}\right). \tag{22}$$

Figure 7 shows a comparison of equation (22) with simulation results. θ_{AB} vanishes for large R/r like $c/2a$, that is

$$\frac{F_{AB}}{mg} \approx \frac{m}{m_{eff}}\left(\frac{r}{R}\right)^3. \tag{23}$$

Of course, F_{AB} must be smaller than the force F_s, up to which stable rest positions on the surface exist (see figure 4). Simple geometry shows that

$$\frac{F_s}{mg} = \sin\gamma_{max} = c^{1/2} \approx \frac{r}{R} \tag{24}$$

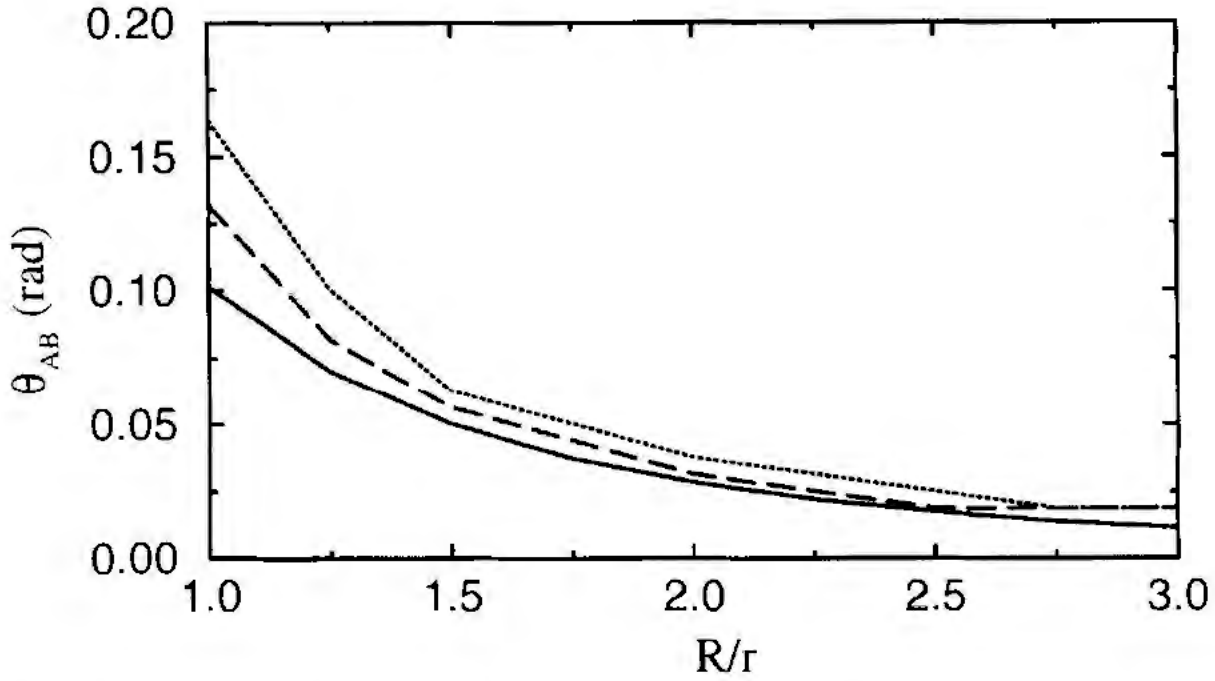

Figure 7. Computation simulations data for $F_{AB} = mg \sin \theta_{AB}$ as a function of R/r for $e_n = 0.7$ (· · · · · ·) and 0.1 (- - - - -): (———) is the analytical result for $e_n = 0$.

§3. Granular packings: dissipation by friction

As in the collisional regime, the quasistatic deformation of granular materials involves both gain (collision) and loss of contacts between particles, which result in the evolution of the contact network and the appearance of an induced anisotropy. However, the average lifetime of contacts is comparable with the macroscopic time scale associated with the global deformation of the system. Owing to the non-smooth character of the Coulomb friction law, at those 'lasting' contacts, the particles may roll upon each other. This is a non-dissipative microscopic mechanism of deformation. If all particles could roll upon one another, then a granular assembly would deform without dissipation. This is, however, forbidden by the frustration of particle rotations (Radjai and Roux 1995). This means that it is impossible for all particles to move and rotate without sliding at some contacts. We see that a granular medium in slow deformation is heterogeneous not only because of the heterogeneous distribution of contact forces, but also owing to the sliding (dissipative) and non-sliding states of contacts. It is our aim here to show that this heterogeneity due to dissipation is correlated with that of the force network.

3.1. *The weak and the strong network of forces*

The numerical study of the statistical distribution of forces in static packings using the contact dynamics approach (Radjai *et al.* 1996) shows that the probability distributions P_F of normal or (absolute values of) tangential forces have two *distinct* parts separated by the average force. The forces lower than the average ('weak' forces) are power law distributed, whereas the higher forces ('strong' forces) have an exponentially decreasing probability:

$$P_f \propto \begin{cases} F^{-\alpha} & F < \langle F \rangle, \\ \exp\left(-\dfrac{\beta F}{\langle F \rangle}\right), & F > \langle F \rangle. \end{cases} \tag{25}$$

We observed the same behaviour also in a simulated granular system under quasistatic biaxial compression (Radjai *et al.* 1997). The absence of a characteristic force in the weak part of the distribution indicates that the weak subnetwork (supporting weak forces) does not directly feel the influence of the deviatoric load. In contrast, the strong forces have a characteristic force set by the external load and the average coordination number.

3.2. *The stress tensors*

What are the respective contributions of the weak and the strong subnetwork to the transmission of forces through the system? The answer to this question needs the investigation of the stress tensor. In a granular system, the stress tensor involves both the contact forces and the contact orientations. It is obtained from (Christoffersen *et al.* 1981) $\sigma_{ij} = V^{-1} \sum_c F_i^c d_j^c$, where the summation is over all contacts and V is the volume of the system. F_i^c is the i component of the total force (normal plus tangential) at the contact c, and d_j^c is the j component of the vector connecting the centres of the contacting particles.

In order to separate the contributions of weak and strong forces to the stress tensor, the summation is to be restricted to contacts in the weak or the strong subnetwork respectively. Figure 8 shows the principal axes and the corresponding eigenvalues of the weak stress tensor $\boldsymbol{\sigma}^{\mathrm{w}}$ and the strong stress tensor $\boldsymbol{\sigma}^{\mathrm{s}}$at the shear peak for the whole sample. The surprising phenomenon observed here is that the weak subnetwork provides a negligibly small contribution to the deviatoric part of the total stress tensor $\boldsymbol{\sigma} = \boldsymbol{\sigma}^{\mathrm{w}} + \boldsymbol{\sigma}^{\mathrm{s}}$, while it represents 28% of the mean pressure. The whole deviatoric load is thus sustained by the strong subnetwork.

The absence of a deviatoric stress is the characteristic property of fluids in static equilibrium. The solids, by contrast, can bear a finite deviatoric stress. In this respect, the weak subnetwork in our system can be viewed as a liquid, whereas the

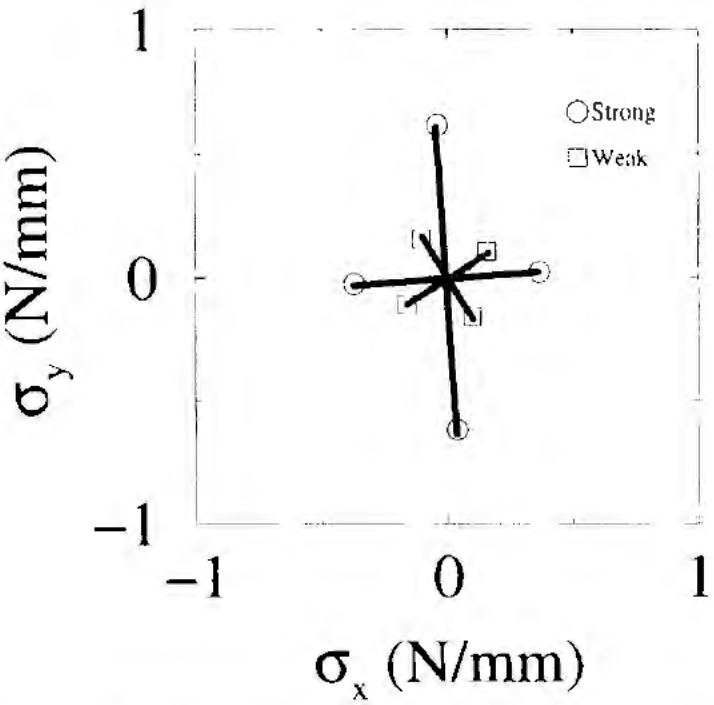

Figure 8. Principal axes and eigenvalues of the stress tensor. The contribution of weak contact forces to the stress tensor is isotropic. The deviatoric stress is transmitted by the strong forces.

strong subnetwork behaves like a solid representing the potential resistance of the medium to shear, a qualitative picture put forward by Cundall and Strack (1983) long ago.

3.3. *The dissipation*

The question which we would like to raise now is how the sliding contacts are distributed with respect to the two networks. In figure 9 we have displayed the two subnetworks and the positions of the sliding contacts. Nearly 8% of contacts are

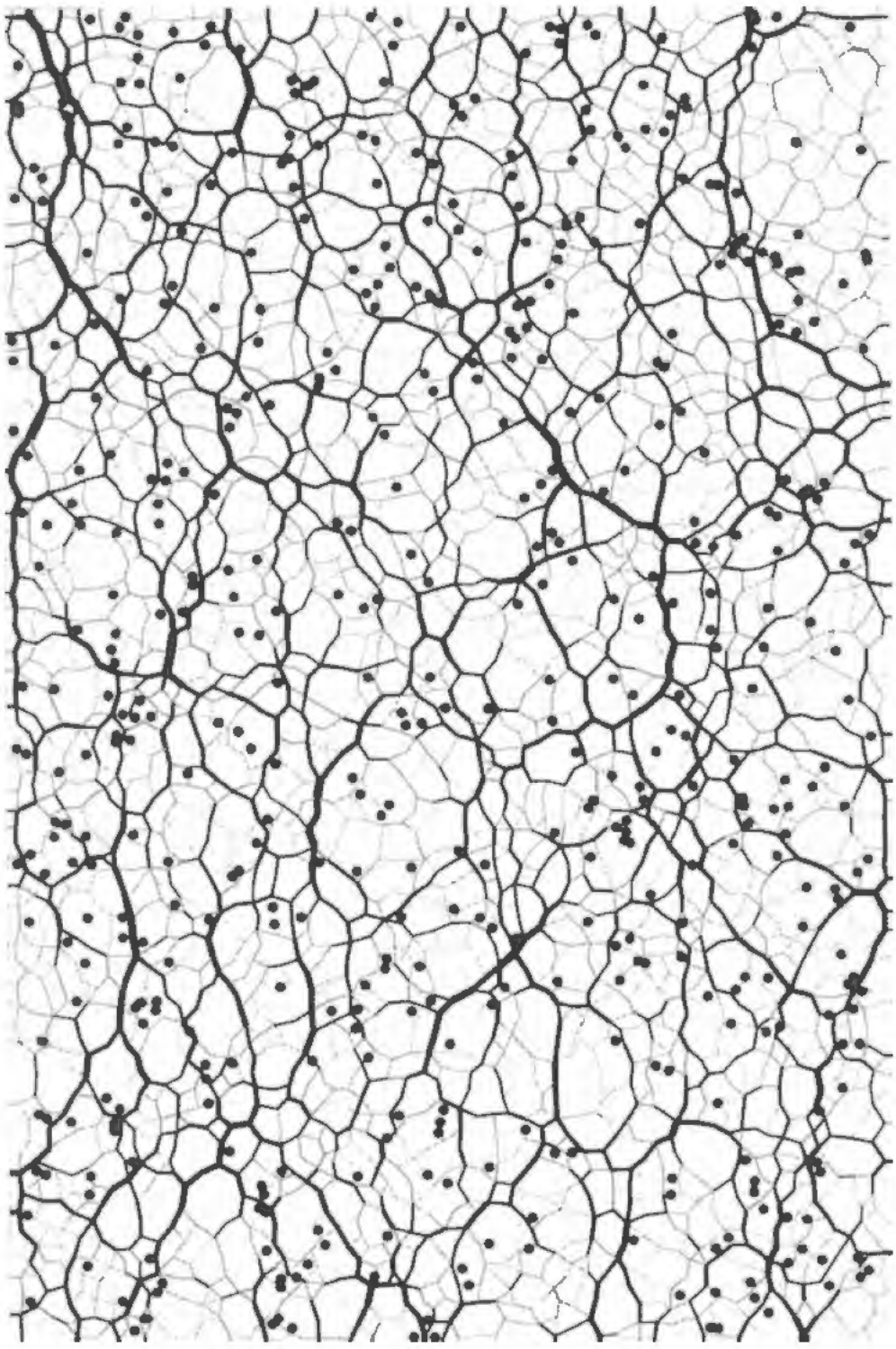

Figure 9. The lines connect the centres of round particles, which are in contact. Bold and light lines indicate contact forces, which are larger, and smaller respectively than the average. Sliding contacts are indicated by full circles.

sliding, and a rapid inspection shows that almost all of them are on the weak subnetwork. This means that the strong contacts are non-sliding, and the whole frictional dissipation takes place within the weak subnetwork.

The friction force at a non-sliding contact is basically a *reaction* force. It ranges from zero to a limit value given by the normal force times the coefficient of friction, and its actual value is a function of all other forces acting on the two contacting particles. According to Coulomb's law of friction, the friction force cannot increase beyond its limit value, and sliding occurs as soon as this limit is reached. These two aspects of friction, reaction force on the one hand and dissipative force on the other hand, appear as complementary behaviours in the strong and weak subnetworks respectively.

Acknowledgement

This paper summarizes work done in collaboration with George Batrouni, Stephan Roux, Jean-Jacques Moreau, Michel Jean with the support of the European Network 'Cooperative Structures in Complex Media'.

APPENDIX

We derive equation (19) for fixed inclination $\theta > \theta_{AB}$ by expanding $\bar{v}$ (equation (16)) in the small variable $c = \sin^2 \gamma_{max}$ (equation (8)). First we expand equation (20):

$$b - \cos\theta = \sin\theta \left(\frac{m_{eff}}{2mc^{1/2}(1-c)} - c^{1/2} \right) + \cos\theta\,[(1-c)^{1/2} - 1] \qquad (A\,1)$$

$$= \sin\theta \left(\frac{m_{eff}}{2m} \frac{1}{c^{1/2}} + \left(\frac{m_{eff}}{2m} - 1 \right) c^{1/2} \right) + O(c). \qquad (A\,2)$$

In leading order the integral (18) can be replaced by the integrand at $\gamma = \theta$:

$$\frac{\bar{v}}{v_0} = (b - \cos\theta)^{1/2}[1 + O(c^{3/2})]. \qquad (A\,3)$$

Substituting equation (A 2) and

$$\frac{m}{r} v_0^2 \sin\theta = \frac{F2m}{m_{eff} c^{1/2}}, \qquad (A\,4)$$

one gets

$$\frac{m}{r} \bar{v}^2 = F\left(\frac{1}{c} + 1 - \frac{2m}{m_{eff}} \right) + O(c^{1/2}). \qquad (A\,5)$$

In order to get the final result (19), one has to insert $c = [r/(R+r)]^2$.

The easiest derivation of equation (22) involves setting $a = A\cos\phi$ and $(1-c)^{1/2} = A\sin\phi$ in equation (20), so that

$$b = A\sin(\theta + \phi), \qquad (A\,6)$$

with

$$A = (a^2 + 1 - c)^{1/2}, \qquad \phi = \tan^{-1}\left(\frac{(1-c)^{1/2}}{a} \right). \qquad (A\,7)$$

Substituting $b = 1$ one finds from equation (A 6) that

$$\theta_{AB} = \sin^{-1}\left(\frac{1}{A}\right) - \phi, \tag{A 8}$$

which is our result (22).

References

Ancey, C., Evesque, P., and Coussot, P., 1996, *J. Phys. Paris, I*, **6**, 725.

Baumberger, T., and Berthoud, P., 1997, *Friction, Arching, Contact Dynamics*, edited by D. E. Wolf and P. Grassberger (Singapore: World Scientific) pp. 3–11.

Christoffersen, J., Mehrabadi, M. M., and Nemat-Nasser, S., 1981, *J. appl. Mech.*, **48**, 339.

Cundall, P. A., and Strack, O. D. L., 1983, *Mechanics of Granular Materials: New Models and Constitutive Relations*, edited by J. T. Jenkins and M. Satake (Amsterdam: Elsevier).

Dippel, S., Batrouni, G. G., and Wolf, D. E., 1996, *Phys. Rev.* E, **54**, 6845; 1997, *ibid.*, **56**, 6845.

Giese, G., and Zippelius, A., 1996, *Phys. Rev.* E, **54**, 4828.

Jaeger, H. M., Nagel, S. E., and Behringer, R. P., 1996, *Rev. mod. Phys.*, **68**, 1259.

McNamara, S., and Young, W. R., 1994, *Phys. Rev.* E, **50**, R28.

Radjai, F., and Roux, S., 1995, *Phys. Rev.* E, **51**, 6177.

Radjai, F., Jean, M., Moreau, J. J., and Roux, S., 1996, *Phys. Rev. Lett.*, **77**, 274.

Radjai, F., Wolf, D., Jean, M., and Moreau, J. J., 1997, *Phys. Rev. Lett.*, in the press.

Ristow, G. H., Riguidel, F.-X., and Bideau, D., 1994, *J. Phys. Paris, I*, **4**, 1161.

Schäfer, J., Dippel, D., and Wolf, D. E., 1966, *J. Phys. Paris, I*, **6**, 5.

Wolf, D. E., 1996, *Computational Physics: Selected Methods—Simple Exercises—Serious Applications*, edited by K. H. Hoffmann, M. Schreiber (Heidelberg: Springer).